Available online at www.sciencedirect.com
SCIENCE DIRECT®
International Journal of Heat and Fluid Flow 25 (2004) 528–536
International Journal of HEAT AND FLUID FLOW
www.elsevier.com/locate/ijhff

Assessment of unsteady RANS in predicting swirl flow instability based on LES and experiments

B. Wegner *, A. Maltsev, C. Schneider, A. Sadiki, A. Dreizler, J. Janicka

Chair of Energy and Powerplant Technology, Department of Mechanical Engineering, Darmstadt University of Technology, Petersenstr. 30, 64287 Darmstadt, Germany

Abstract

Swirl flows play an important role in many engineering applications such as modern gas turbines, aero propulsion systems etc. While the enhanced mixing and stabilisation of the flame caused by the swirl are desirable features, such flows often exhibit hydrodynamic instabilities called precessing vortex core. For design purposes it is very important to predict such instabilities. Computational fluid dynamics (CFD) using Reynolds-averaged Navier–Stokes (RANS) type turbulence models are state of the art for the prediction of flow properties in engineering practice. The objective of this paper is therefore to evaluate the performance of the unsteady RANS (U-RANS) method in predicting the precessing vortex core phenomenon. To this end, an unconfined swirling flow with precessing vortex core at swirl number 0.75 and Reynolds number ranging from 10 000 to 42 000, investigated by means of both experiments and large eddy simulation, is utilised. The results show that U-RANS is able to capture the precessing vortex core both qualitatively and in parts quantitatively.

Keywords: Unsteady flow; U-RANS modelling; Swirl; Precessing vortex core

1. Introduction

Swirling motion in fluid flow has been used for many decades in a broad range of engineering applications. Many studies have been performed on swirl-burners due to their widespread use in combustion systems. In these systems, enhanced mixing and stabilisation of the flame are beneficial phenomena associated with swirl. Reviews on the topic have been given by Syred and Beer (1974), Leibovich (1978), Gupta et al. (1984) and recently by Lucca-Negro and O'Doherty (2001). Chanaud (1965) reported periodic vortex instabilities associated with the swirl in a certain regime of Reynolds and swirl numbers. Since then the so called precessing vortex core (PVC) phenomenon has been paid much attention. It has been observed in premixed combustion systems that the oscillations of the precessing vortex core can amplify and cause a feedback mechanism with acoustic modes of the system. This poses a problem as lean premixed combustion is becoming more and more popular due to it's potential of low-NO_x production. Therefore models and simulation methods used in combustor design must be able to predict the precessing vortex core.

For the numerical prediction of flow properties in engineering practice RANS type turbulence models are state of the art. This is mostly motivated by reasonable computational costs required by this method. A review on the application of RANS models to swirl flows has been given by Sloan et al. (1986). Many studies have shown that the standard k–ε and other linear two-equation models in general perform poor due to their deficiencies in the presence of strong streamline curvature. To overcome this weakness a whole category of non-linear eddy-viscosity models (NLEVMs) has emerged at an intermediate level of complexity (e.g. Shih (1996) or Craft et al. (1996)). The inversion of algebraic forms of the Reynolds stress-transport equations to yield explicit forms (EARSMs) relating non-linearly the Reynolds stresses to strain and vorticity (Gatski and Speziale (1993), Jongen and Gatski (1998)) leads today to an efficient modelling that in general is able of capturing swirled flows at the first order closure level. Improvements related to strong swirl or streamline

* Corresponding author. Tel.: +49-6151-162-357; fax: +49-6151-166-555.
E-mail address: bwegner@ekt.tu-darmstadt.de (B. Wegner).

0142-727X/$ - see front matter © 2004 Elsevier Inc. All rights reserved.
doi:10.1016/j.ijheatfluidflow.2004.02.019

curvature have also been reported (e.g. Wallin et al. (2003)). Putting aside some novel developments (Kassinos et al. (2000), Sadiki et al. (2003) etc.), the most complex closure forms are based on solving directly the conventional transport equations for the Reynolds stresses. Full Reynolds stress models (RSM) are recently being improved by new models for the redistributive pressure–strain and the dissipative processes as well as through a detailed attention to modelling the effects of non-equilibrium, viscosity and wall blockage on the turbulence in the near-wall layer. For a recent review on RANS/U-RANS in general (see Durbin, 2002).

Most RANS computations of swirl flows in the past have been performed assuming axisymmetry and therefore using 2D computational grids. Since swirl flow instabilities are three-dimensional and time dependent in nature, their numerical prediction is computationally expensive and has been attempted only recently. Bowen et al. (1998) achieved qualitative agreement with experimental data for a swirl-burner furnace system using a Reynolds stress model. They set asymmetric initial conditions from which the PVC ensued, but was damped out after a few revolutions. The precession frequency was predicted within 20% of the value observed in experiments. Guo et al. (2002) employed a k–ε-model to a low-swirl flow in a sudden expansion chamber. They observed several modes of vortex core oscillation. A comparison with experimental results was not given in this work.

In the last few years, large eddy simulation (LES) has been successfully used by several authors to predict swirling flows with or without unsteady phenomena. Pierce and Moin (1998) achieved excellent results in predicting swirled coaxial jets. Derksen and den Akker (2000) accurately captured the PVC phenomenon performing LES of a cyclone. Recently, Tang et al. (2002) obtained encouraging results applying LES to the simulation of an isothermal swirl flow with re-circulation. Düsing et al. (2002) used LES to investigate the influence of oscillating inflow conditions on a swirled, non-premixed combustor. This motivates the use of LES results for validation purposes in U-RANS modelling besides experimental data or where such data are not available.

In LES, the stochastic nature of the solution is retained by performing a low-pass filtering instead of some kind of averaging of the flow field. Hence, Reynolds averaged statistics must be evaluated by accumulating a large enough sample number. As pointed out by Iaccarino et al. (2003) the time-step requirements of U-RANS and LES are quite different. Whilst LES resolves the eddies of the turbulence itself, unsteady RANS models the turbulence and resolves only unsteady mean flow structures. Consequently, LES typically requires much higher temporal resolution, and is more costly. It also requires a long integration time to build an ensemble averaged solution. In U-RANS, just a few periods of the unsteadiness have to be computed since the solution is of deterministic nature. Regarding the modelling issues discussed above, unsteady RANS is expected to be less reliable than classical LES, but it will require significantly less computation time. It is therefore a potentially suitable technique for industrial applications.

The present study focuses on an evaluation of the performance of U-RANS simulations in predicting an unconfined swirling flow with a processing vortex core. The flow under consideration has been studied in house by means of experiments which are complemented by LES of the same configuration.

2. Modelling and computational method

For both the U-RANS and the LES approach the time dependent three dimensional continuity and Navier–Stokes equations are considered for the incompressible case

$$\frac{\partial \bar{u}_i}{\partial x_i} = 0 \tag{1}$$

$$\frac{D\bar{u}_i}{Dt} = \frac{\partial}{\partial x_j}\left(\bar{\nu}\frac{\partial \bar{u}_i}{\partial x_j} - \tau_{ij}\right) - \frac{1}{\varrho}\frac{\partial \bar{p}}{\partial x_i} \tag{2}$$

The overbar denotes the Reynolds averaging and spatial filtering operators for the U-RANS and LES respectively. The turbulent stress tensor τ_{ij} appearing as an unclosed term on the r.h.s. of Eq. (2) has to be modelled. In the frame work of RANS $\tau_{ij} = \overline{u_i' u_j'}$ is called the Reynolds stress tensor whereas it is called the subgrid-scale stress tensor defined as $\tau_{ij} = \overline{u_i u_j} - \bar{u}_i \bar{u}_j$ for LES.

2.1. U-RANS modelling

Besides the modelling question discussed in the introduction, a more fundamental debate is currently going on about the applicability of the RANS modelling approach to unsteady problems. It has been claimed in the past that RANS cannot be applied to unsteady flows unless there is a *spectral gap* between the unsteadiness and the turbulence. This is based on the understanding that Reynolds averaging equals temporal averaging. In this spirit, to capture a periodic unsteadiness in the mean flow using U-RANS, the averaging period should be much smaller than the time scale of the unsteady mean motion. At the same time, the time period should be orders of magnitude higher than the time scale of the random fluctuations for the averaging to make sense. As pointed out by Durbin (2002) it is a misconception that Reynolds averaging equals temporal averaging. If statistical periodicity is defined via the existence of a narrow peak representing the unsteadiness of the flow in the

spectrum there is no need for a spectral gap. The peak can occur right in the midst of the broadband turbulent scales and Reynolds averaging is simply interpreted as ensemble or phase averaging. On the other hand, if the unsteady coherent motion creates a strong disequilibrium, the assumptions underlying standard RANS closures might not be sufficient anymore. In this case it might be necessary to incorporate some kind of spectral information into the model, e.g. by using two-time-scale models as proposed by Hanjalic et al. (1980).

In the present work, first simulations were performed using a standard k–ε-model, solving the unsteady governing equations. These simulations showed some periodic behavior in an early stage, but as the simulations went on, the instability decayed and a steady state solution was finally reached. This is the same phenomenon as observed earlier by Bowen et al. (1998). Hence, a second-order closure was chosen for it's well-known capability to well predict swirl flows. To this end, the transport equations for the components of the Reynolds stress tensor have to be solved.

$$\frac{D\overline{u_i'u_j'}}{Dt} = \underbrace{\frac{\partial}{\partial x_k}\left(-\overline{u_k'u_i'u_j'} - \frac{1}{\varrho}\overline{p'u_i'}\delta_{jk} - \frac{1}{\varrho}\overline{p'u_j'}\delta_{ik}\right)}_{T_{ijk}} - \underbrace{\left(\overline{u_i'u_k'}\frac{\partial \bar{u}_j}{\partial x_k} + \overline{u_j'u_k'}\frac{\partial \bar{u}_i}{\partial x_k}\right)}_{P_{ij}} + \underbrace{\overline{\frac{p'}{\varrho}\left(\frac{\partial u_i'}{\partial x_j} + \frac{\partial u_i'}{\partial x_j}\right)}}_{\Pi_{ij}} - \underbrace{2\nu\overline{\frac{\partial u_i'}{\partial x_k}\frac{\partial u_j'}{\partial x_k}}}_{\varepsilon_{ij}} \tag{3}$$

For the turbulent transport term T_{ijk} the model of Shir (1973) is applied.

$$T_{ijk} = \frac{\partial}{\partial x_k}\left(C_s\frac{k^2}{\varepsilon}\frac{\partial \overline{u_i'u_j'}}{\partial x_k}\right) \tag{4}$$

The production term P_{ij} does not contain any unclosed expressions. The linear model of Jones (1994) is applied to model the pressure-strain correlation tensor Π_{ij}.

$$\Pi_{ij} = -2C_1\varepsilon\left(\frac{\overline{u_i'u_j'}}{k} - \frac{2}{3}\delta_{ij}\right) + C_2\overline{u_k'u_l'}\frac{\partial \bar{u}_k}{\partial x_l} + C_3\left(\overline{u_j'u_k'}\frac{\partial \bar{u}_i}{\partial x_k} + \overline{u_i'u_k'}\frac{\partial \bar{u}_j}{\partial x_k}\right) + C_4k\left(\frac{\partial \bar{u}_i}{\partial x_j} + \frac{\partial \bar{u}_j}{\partial x_i}\right) - \left(\frac{3}{2}C_2 + C_3\right)\left(\overline{u_j'u_k'}\frac{\partial \bar{u}_k}{\partial x_i} + \overline{u_i'u_k'}\frac{\partial \bar{u}_k}{\partial x_j}\right) \tag{5}$$

The dissipation tensor ε_{ij} in (3) is modelled by assuming local isotropy of the small scales.

$$\varepsilon_{ij} = \frac{2}{3}\varepsilon\delta_{ij} \tag{6}$$

Table 1
Model constants for the RSM

C_1	C_2	C_3	C_4	C_S	$C_{\varepsilon 1}$	$C_{\varepsilon 2}$
3.0	−0.44	0.46	−0.23	0.1	1.4	1.9

where a separate transport equation is solved for ε (Jones (1994)).

$$\frac{\partial \varepsilon}{\partial t} + \frac{\partial}{\partial x_j}(\bar{u}_j\varepsilon) = \frac{\partial}{\partial x_j}\left(C_s\frac{k^2}{\varepsilon}\frac{\partial \varepsilon}{\partial x_j}\right) - C_{\varepsilon 1}\frac{\varepsilon}{k}\overline{u_i'u_j'}\frac{\partial \bar{u}_i}{\partial x_j} - C_{\varepsilon 2}\frac{\varepsilon^2}{k} \tag{7}$$

The values of the model constants used in the closure procedure described above are listed in Table 1.

For near wall treatment the logarithmic law of the wall has been employed in conjunction with an explicit setting of the Reynolds stress anisotropy at the wall based on experimental data.

Other RSM were also tried out in the course of this investigation, but no systematic study of model behavior has been performed though yet. For further details on the RANS modelling the reader is referred to Maltsev (2003).

2.2. LES modelling

For the LES a Smagorinsky-model with dynamic procedure according to Lilly (1992) was used to describe the influence of the small scales on the resolved ones. The filtering operation is performed implicitly by means of the finite-volume discretisation. No special wall-treatment is included in the subgrid-scale model. We rather rely on the ability of the dynamic procedure to capture the correct asymptotic behavior of the turbulent flow when approaching the wall (see e.g. Lesieur and Métais, 1996).

2.3. Computational method

The same CFD code was used for both U-RANS and LES calculations. The governing equations were discretised on a block-structured boundary-fitted collocated grid following the finite-volume approach. Spatial discretisations are *2nd* order with a flux blending technique for the convective terms. The solution is forwarded in time using the *2nd* order accurate implicit Crank–Nicolson scheme. A SIMPLE type pressure correction method is used for pressure–velocity coupling. The resulting set of linear equations are solved iteratively. Details on the method can be found in the paper by Durst and Schäfer (1996).

For the U-RANS computations, a flux blending parameter $\alpha = 0.5$ (i.e. 50% 1st order upwind differencing) was first used to ensure stability of simulations. After the simulations had evolved, the flux blending parameter could be increased up to $\alpha = 0.9$, thus

reducing the upwind contribution to 10%. All the LES were run with almost pure central differencing ($\alpha = 0.95$). The time step width was chosen to give a CFL number of the order of five for the U-RANS. For the LES the time step width was smaller by a factor of 10 to resolve all turbulent fluctuations down to the grid-scale eddies.

3. Experimental and numerical setup

The flow configuration investigated in this paper is based on a non-premixed swirl-burner that has been extensively studied in the well-known TECFLAM-project (see e.g. Schneider et al. (2001)). Recently, the setup has been changed to investigate length and time scales in premixed combustion. A set of isothermal air flow measurements have also been performed in the course of this investigation which are used within this paper.

The experimental setup consists of a movable block type swirler which feeds an annulus from which the air flow enters the measurement section at ambient pressure and temperature. The Reynolds number is computed based on the bulk velocity and bluff-body diameter. Three cases were investigated experimentally in which the (geometrical) swirl number was set to $S = 0.75$. Two cases were selected for this paper which will be referred to as the 30 and 150 kW cases (according to the thermal power for premixed operation of the burner). The Reynolds numbers Re and mass flow rates $\dot{V}$ of the two cases are given in Table 2.

A coflow of 0.5 m/s surrounds the swirler device. A sketch of the device is given in Fig. 1. Single-point measurements were performed with a TSI 2d-LDV setup that was used in backscatter mode to determine two velocity components at a time. Magnesium oxide particles of less than 1 μm diameter were used to seed the flow. For the evaluation of mean values and fluctuations roughly 10 000 events were sampled. The overall error for the experimental data is estimated to be within 3% for the mean values and 7% for fluctuations. Two-point measurements were also performed where one probe was kept fixed while the other probe was traversed. All the samples collected with the fixed probe (a total of 1.5×10^6) went into the computation of the temporal autocorrelation and power spectral density which was used to determine the vortex core frequency. The two-point correlations computed from the data collected thus are not presented in this paper.

Table 2
The two cases investigated in this paper

	30 kW	150 kW
Re	10 000	42 000
$\dot{V}$ (m^3/h)	35.54	174.55

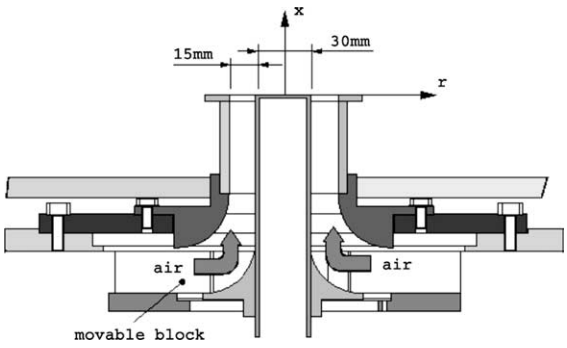

Fig. 1. Sketch of the movable block swirler device and dimensions (in mm). The coordinate system used throughout the rest of the paper is attached to the centre of the bluff-body surface.

The computational domain was shaped cylindrically being 600 mm long with a diameter of 600 mm. Free slip boundary conditions were applied to the lateral boundaries and a zero gradient outflow condition was set for the face surface. First simulations were performed with the inlet boundary being flush with the swirler exit plane, prescribing experimental data taken at 1 mm above the swirler exit as inlet boundary conditions. No instable behavior could be obtained though by doing so. Therefore the swirler device was included in the computational domain. Hence, the inlet boundary was moved to the inlet channels of the swirler device. The swirler was first resolved with 8 cells in the radial direction resulting in a grid with a total of ≈500 000 cells. After doing so, an unstable behavior of the expected kind was observed in the simulations, but due to unsatisfactory results in the near-nozzle region the resolution of the swirler was then doubled to 16 points in the radial direction. This increased the total number of grid points to ≈800 000. A picture of the grid that was used to model the swirler is given in Fig. 2.

Since the swirler device is fed from a plenum chamber, a constant radial inflow velocity was set on the inlet boundary which was adjusted to result in the correct mass flow for the two cases.

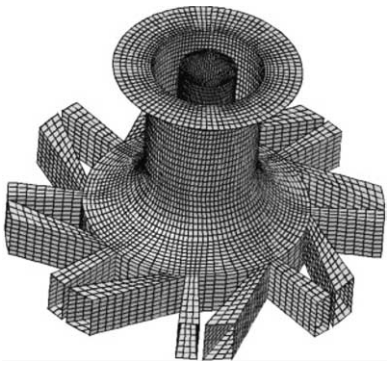

Fig. 2. The computational grid used to model the movable block swirler device.

4. Results and discussion

4.1. Flow structure

Due to the single-point nature of the LDV technique, no information about instantaneous flow structures could be obtained from the experimental data. This kind of information can be obtained from the LES. Fig. 3 shows instantaneous snapshots from the LES flow field covering one revolution of the precessing vortex core. The flow features that can be observed are:

- The central reverse flow zone performs a precession motion around the bluff-body of the swirler device.
- The recirculation reaches upstream into the swirler device. This explains why the first simulations performed without the swirler failed to predict any unsteady behavior of the flow.
- Two opposed helical vortices shed off the outside edge of the swirler exit. They rotate with the same frequency as the recirculation bubble.

As is shown by Fig. 4, the U-RANS clearly captures the precessing vortex core: a rotating movement of the vortex centre about the system's geometrical axis can be observed. It is noteworthy that no converged stationary solution could be obtained which also indicates the unsteady nature of the flow under consideration. When comparing the U-RANS results to phase averaged LES data both methods show the same qualitative overall flow behavior (Fig. 5). The reader should not get irritated from the different spacing and number of the vectors in Figs. 4 and 5. The vectors from the U-RANS are plotted directly at the grid nodes while the LES data were interpolated to a coarser grid on which the phase averaging was performed in a post processing step.

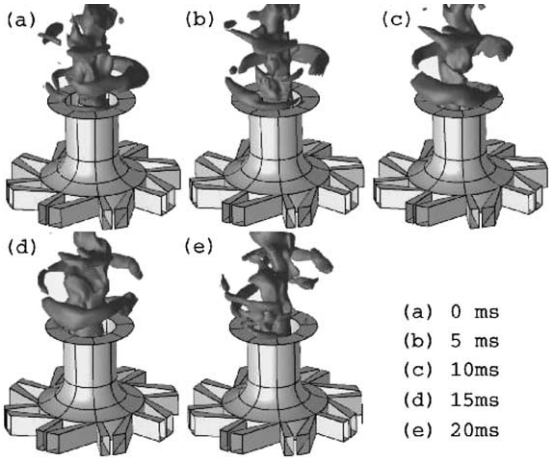

Fig. 3. Isosurfaces of instantaneous axial velocity $u = -0.5$ m/s taken from the LES of case 30 kW showing the flow structure covering one revolution of the vortex core (taken from Wegner et al. (2004)).

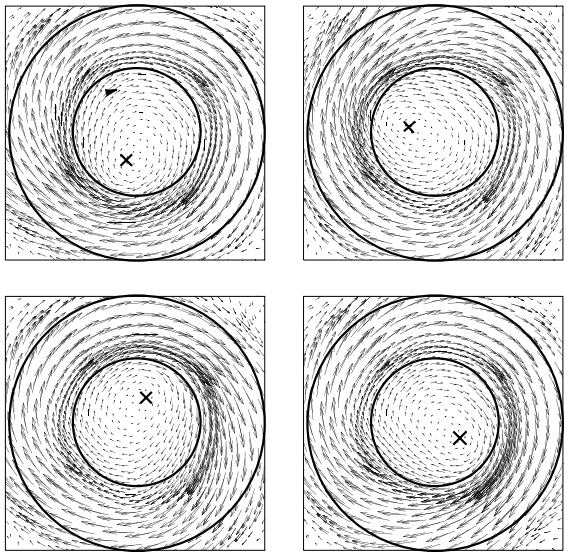

Fig. 4. Sequence of snapshots (top left to bottom right) taken from the U-RANS of the 30 kW case showing vector plots of velocity in a plane $x = 30$ mm. The swirler annulus is indicated by the two concentric circles. The approximate instantaneous vortex centre and precession direction are also indicated.

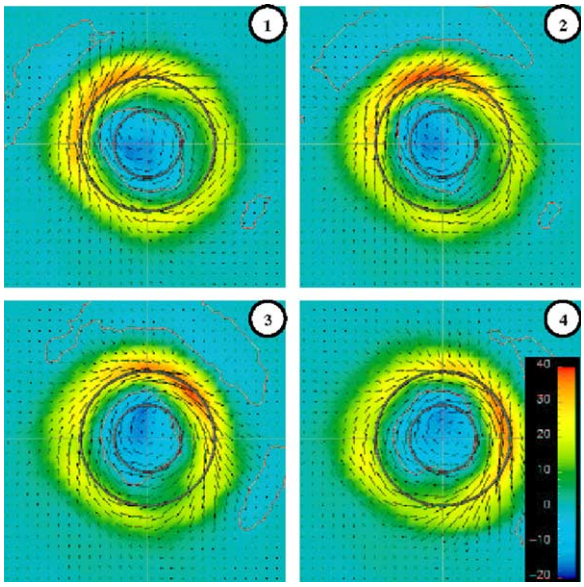

Fig. 5. Plot of phase averaged velocity vectors from the LES (30 kW case) in a plane $x = 30$ mm, confirming the structure seen in the U-RANS (Fig. 4).

5. Velocity and fluctuation profiles

Radial profiles of time averaged axial and azimuthal velocity as well as the turbulent kinetic energy for both cases are shown in Figs. 6–11. Both LES and U-RANS simulations capture the experimental mean velocity profiles quite well. Near the swirler exit the RSM gives even better results than the LES. Since the RSM in-

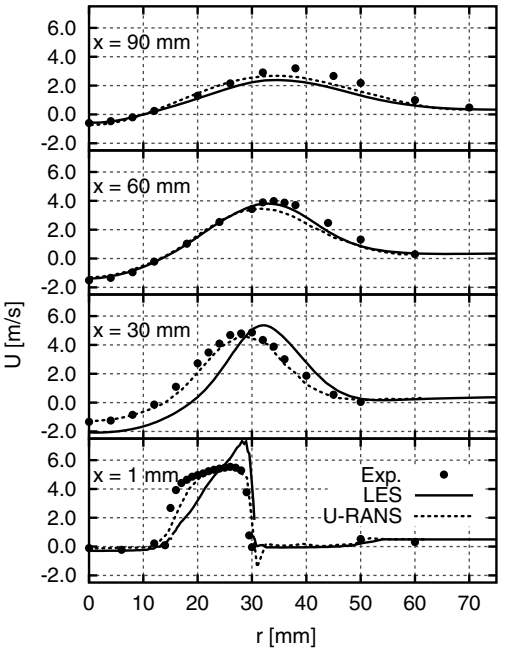

Fig. 6. Radial profiles of time averaged axial velocity at several axial positions for the 30 kW case.

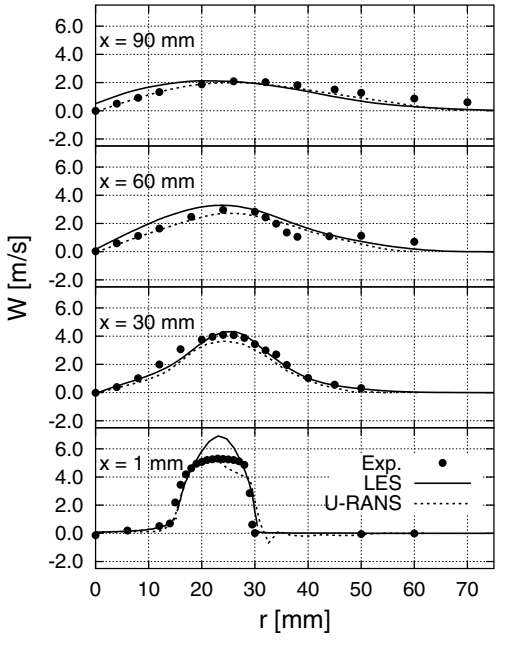

Fig. 7. Radial profiles of time averaged azimuthal velocity at several axial positions for the 30 kW case.

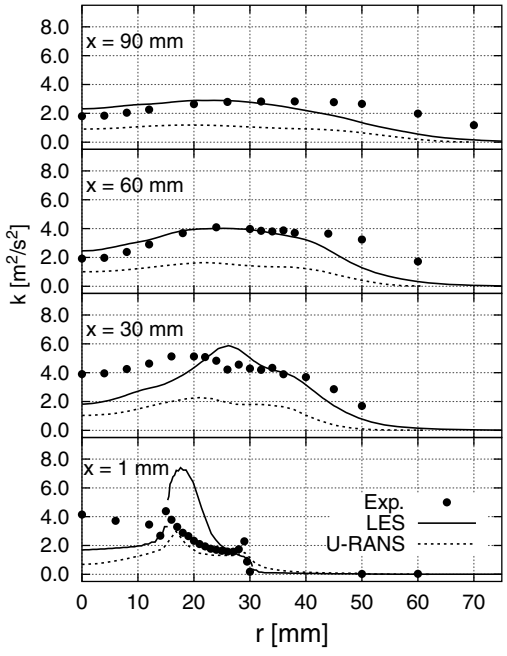

Fig. 8. Radial profiles of time averaged total kinetic energy at several axial positions for the 30 kW case.

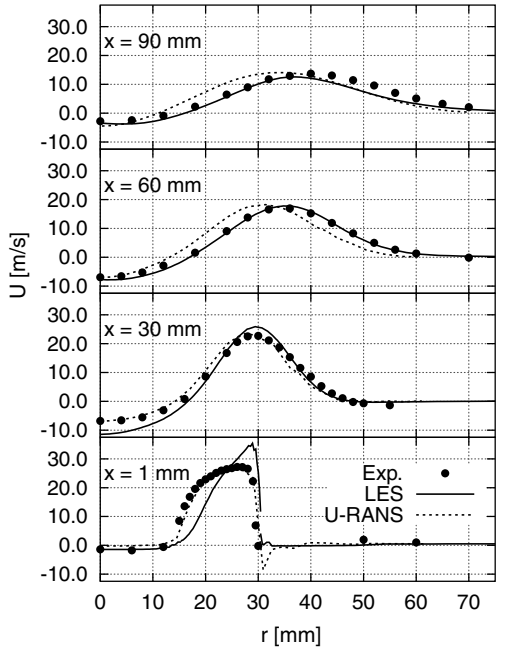

Fig. 9. Radial profiles of time averaged axial velocity at several axial positions for the 150 kW case.

cludes a wall-model it has got an advantage in predicting the wall-dominated flow in the swirler device. The unsatisfactory accuracy of the LES results at the swirler exit can be explained by the relatively coarse grid resolution in the swirler device. Only 16 cells were used to resolve the radial direction of the annulus. This is by far not fine enough for the LES to cover the near wall behavior of the flow. The plots of kinetic energy support this as the peak fluctuations at the swirler exit are located in the annulus middle. Due to the wall-induced shear there should be fluctuation peaks near the wall. In order to overcome this problem, more LES computations would be necessary performed with an increased resolution in the swirler.

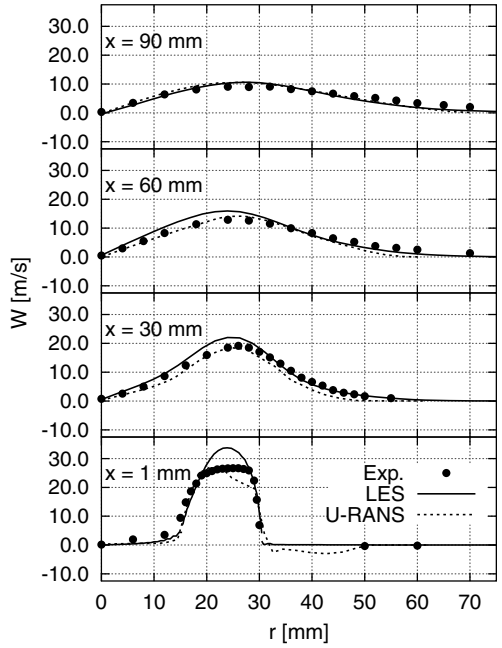

Fig. 10. Radial profiles of time averaged azimuthal velocity at several axial positions for the 150 kW case.

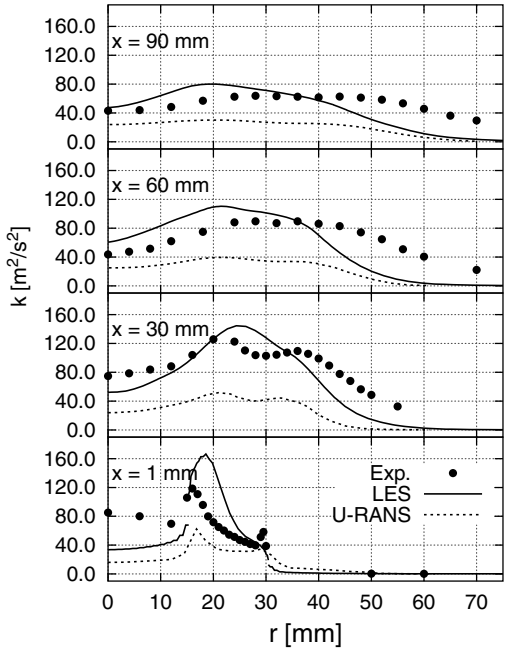

Fig. 11. Radial profiles of time averaged total kinetic energy at several axial positions for the 150 kW case.

Though the shape of the profiles obtained with the U-RANS for the total kinetic energy (Figs. 8 and 11) is quite good, the level of energy is much too low when compared to the experiments. This was found to be much worse in the first computations with lower flux-blending parameters, indicating a significant influence of numerics on the U-RANS results. The LES gives the same level of kinetic energy as the experiments and also captures a good deal of the profile shapes. In the U-RANS framework, kinetic energy denotes the sum of the modelled turbulent kinetic energy $k = 1/2 \cdot \overline{u_i' u_i'}$ and the resolved energy contained in the unsteady flow motion. When comparing velocity time series from the U-RANS to phase averaged time series from the LES, it was found that the amplitude of the coherent velocity fluctuation was much too low in the U-RANS. Hence, the resolved energy is underpredicted by the unsteady RANS.

As the plots of axial velocity indicate (Figs. 6 and 9), the length and width of the recirculation zone is quite well-predicted by the U-RANS.

5.1. Precession frequency

For both the experiment and the LES, the vortex core precession frequency was obtained from the turbulent energy spectrum as computed from temporal autocorrelations. As can be seen in Fig. 12 the spectra show distinct peaks associated with the motion of the vortex core. Furthermore, these spectra show a second weaker peak at the doubled PVC frequency. This peak is associated with the opposed helical vortices that are shown by the LES. Since they perform a rotating motion at the same speed as the central recirculation, the monitoring point (at which the velocity time series for the spectral analysis was sampled) is passed twice by such a structure in one PVC cycle. Hence the doubled frequency. As far as the position of the peak frequency in the turbulent spectrum is concerned, it seems that the coherent motion is associated to rather large frequencies. From the temporal autocorrelations of both the LES and the experiments, a factor of approximately five was estimated between the precession period τ and the integral time scale T. This implies that the coherent and turbulent scales are separated from each other.

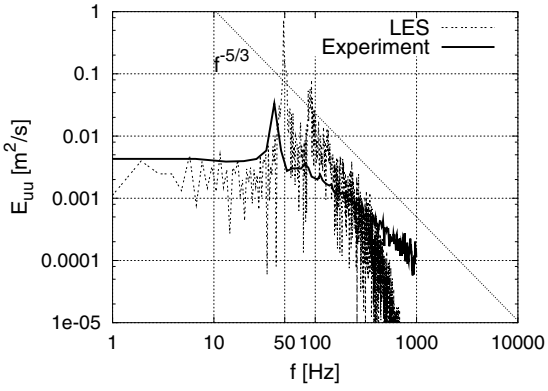

Fig. 12. Turbulent energy spectra computed from temporal autocorrelations at $x = 1$ mm, $r = 20$ mm obtained from the experiments and LES of the 30 kW case. The dotted line indicates the $f^{-5/3}$ decay of energy.

Since computation of a turbulent energy spectrum is not possible for the U-RANS (no two-point information is available), velocity time series recorded at selected points of the flow field were Fourier transformed directly. The result of this procedure is shown in Fig. 13. For the Fourier analysis of the U-RANS, the spectral resolution was quite coarse (≈10% when related to the peak frequency). This is due to the fact that only two vortex core periods were analysed. But within that range of uncertainty the precession frequencies are predicted with remarkable accuracy when compared to the experimental data. The precession frequency can also be expressed in terms of the Strouhal number defined as $St = L/\tau \cdot U$, where τ is the inverse of the peak frequency and the characteristic velocity U and length L are the same as were used for computing the Reynolds number. In Fig. 14, the Strouhal numbers corresponding to the peak frequency for the two cases are plotted as a function of Reynolds number.

For a given flow configuration the Strouhal number is expected to reach an asymptotic value in the limit of high Reynolds numbers. The precession frequency then increases linearly with the flow rate (Gupta et al. (1984)).

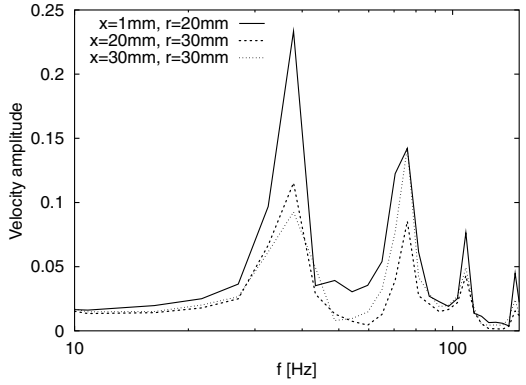

Fig. 13. Fourier transform of velocity from the U-RANS of the 30 kW case.

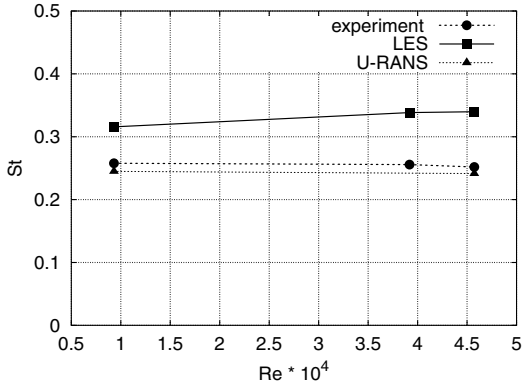

Fig. 14. Dimensionless peak precessing vortex core frequency plotted over Reynolds number.

This behavior seems to be correctly captured by the U-RANS. It can be seen that the frequencies obtained from the LES are about 20% higher than those from U-RANS and experiments. This is clearly related to the inexact prediction of velocity profiles in the swirler annulus. In the plots of mean tangential velocity (Figs. 7 and 10), at $x = 1$ mm one can see that the LES over-predicts the tangential velocity component. When computing the effective swirl number it was found that in the LES it is about 10–15% higher than in the experiment. This in turn is likely responsible for the over-prediction of the precession frequency which is a function of the swirl number.

6. Conclusions

So far it could be confirmed that the U-RANS method employing a full Reynolds stress model is able to capture the precessing vortex core phenomenon both qualitatively and in parts also quantitatively. Good agreement of mean velocities was achieved when comparing the U-RANS results to experimental data and LES computations. A remarkable accuracy was achieved in predicting the vortex core precession frequency. On the other hand, the energy contained in the coherent motion of the PVC was significantly under-predicted by the unsteady RANS. The reason for this is not clear yet, but the amount of numerical dissipation contained in the discretisation scheme seems to play an important role. Furthermore, although it is justified to speak of at least a weak scale separation in the flow considered here, it might still be necessary to take into account disequilibrium effects as discussed above. This is an issue requiring further investigation.

It should be mentioned that for 3D time-dependent simulations as performed in the present study the computational cost is significantly increased when compared to steady state RANS computations. The use of algebraic Reynolds stress models instead of the differential model used in this paper might prove useful in this regard, but is left as future work. Computational requirements are still low when compared with those for LES. To perform a more accurate LES, a finer mesh should be used in the wall-dominated swirler device. So far LES is very good for flow systems, where the flow is governed by large, turbulent structures, which can be captured by a fairly coarse mesh. However, if attached boundary layers are important, LES will probably give partially dissatisfying predictions in these regions (see Swirl number!), unless fine grids are used. Besides an appropriate near-wall SGS-modelling (Piomelli et al. (2002)) to get around this bottleneck of LES near walls, many researchers (see Durbin (2002)) suggest hybrid LES-RANS methods, in which RANS is used near the wall while LES is utilized in the remaining part of the

domain. However, the interface coupling remains the main point of issue (Spalart (2000)).

Acknowledgements

The authors gratefully acknowledge the *Deutsche Forschungsgemeinschaft* for financial support through SFB 568 ''Flow and Combustion in Future Gas Turbine Combustion Chambers'' and through GK 91 ''Modellierung und numerische Beschreibung technischer Strömungen''.

References

Bowen, P., O'Doherty, T., Lucca-Negro, O., 1998. Rotating instabilities in swirling and cyclonic flows, Part B: Theoretical Analysis. In: Zhang, D., Nathan, G. (Eds.), Thermal Energy Engineering and the Environment. Department of Chemical Engineering, The University of Adelaide, Adelaide, pp. 197–220.

Chanaud, R., 1965. Observations of oscillatory motion in certain swirling flows. J. Fluid Mech. 21 (1), 111–127.

Craft, T., Launder, B., Suga, K., 1996. Development and applications of a cubic eddy viscosity model of turbulence. Int. J. Heat Fluid Flow 17 (2), 108–115.

Derksen, J., den Akker, H.V., 2000. Simulation of vortex core precession in a reverse-flow cyclone. AIChE J. 46 (7), 1317–1331.

Durbin, P., 2002. A perspective on recent developments in RANS modeling. In: Rodi, W., Fueyo, N. (Eds.), Engineering Turbulence Modelling and Experiments 5. Elsevier Science Ltd., pp. 3–16.

Durst, F., Schäfer, M., 1996. A parallel block-structured multigrid method for the prediction of incompressible flow. Int. J. Num. Meth. Fluids 22, 549–565.

Düsing, M., Sadiki, A., Janicka, J., 2002. LES of confined methane-air diffusion flames using oscillating inflow conditions. In: Rodi, W., Fueyo, N. (Eds.), Engineering Turbulence Modelling and Experiments 5. Elsevier Science Ltd., pp. 907–926.

Gatski, T., Speziale, C., 1993. On explicit algebraic stress models for complex turbulent flows. J. Fluid Mech. 254, 59–78.

Guo, B., Langrish, T., Fletcher, D., 2002. CFD simulation of precession in sudden pipe expansion flows with low inlet swirl. Appl. Math. Modell. 26, 1–15.

Gupta, A., Lilley, D., Syred, N., 1984. Swirl Flows. Abacus Press, Tunbridge Wells, Kent.

Hanjalic, K., Launder, B., Schiestel, R., 1980. Multiple time-scale concepts in turbulent transport modelling. In: Bradbury, L., Durst, F., Launder, B., Schmidt, F., Whitelaw, J. (Eds.), Turbulent Shear Flows 2. Springer-Verlag, Berlin, pp. 36–49.

Iaccarino, G., Ooi, A., Durbin, P., Behnia, M., 2003. Reynolds averaged simulation of unsteady separated flow. Int. J. Heat Fluid Flow 24 (2), 147–156.

Jones, W.-P., 1994. Turbulence modeling and numerical solution methods for variable density flows. In: Libby, P., Williams, F. (Eds.), Turbulent Reacting Flows. Academic Press, London, San Diego, New York, pp. 309–347.

Jongen, T., Gatski, T., 1998. General explicit algebraic stress relations and best approximations for three dimensional flows. Int. J. Eng. Sci. 36, 739–763.

Kassinos, S., Langer, C., Haire, S., Reynolds, W., 2000. Structure-based turbulence modeling for wall-bounded flows. Int. J. Heat Fluid Flow 21 (5), 599–605.

Leibovich, S., 1978. The structure of vortex breakdown. Annu. Rev. Fluid Mech. 10, 221–246.

Lesieur, M., Métais, O., 1996. New trends in large eddy simulation of turbulence. Annu. Rev. Fluid Mech. 28, 45–82.

Lilly, D., 1992. A proposed modification of the germano subgrid-scale closure method. Phys. Fluids 4 (3), 633–635.

Lucca-Negro, O., O'Doherty, T., 2001. Vortex breakdown: a review. Prog., Energ. Combust. Sci. 27 (4), 431–481.

Maltsev, A., 2003. Towards the development and assessment of complete CFD models for the simulation of stationary gas turbine combustion processes, Ph.D. thesis, Darmstadt University of Technology.

Pierce, C., Moin, P., 1998. A dynamic model for subgrid-scale variance and dissipation rate of a conserved scalar. Phys. Fluids 10 (12), 3041–3044.

Piomelli, U., Balaras, E., Squires, K., Spalart, P., 2002. Interaction of the inner and outer layers in large-eddy simulation with wall-layer models. In: Rodi, W., Fueyo, N. (Eds.), Engineering Turbulence Modelling and Experiments 5. Elsevier Science Ltd., pp. 307–316.

Sadiki, A., Jakirlic, S., Hanjalic, K., 2003. Towards a thermodynamically consistent, anisotropy-resolving turbulence model for conjugate flow, heat and mass transfer. In: Turbulence, Heat and Mass Transfer, vol. 4. pp. 545–552.

Schneider, C., Repp, S., Sadiki, A., Dreizler, A., Janicka, J., 2001. The effect of swirling number variation on turbulent transport and mixing processes in swirling recirculating flows: experimental and numerical investigations. In: Second International Symposium on Turbulence and Shear Flow Phenomena, vol. 3. pp. 363–368.

Shih, T., 1996. Constitutive relations and realizability of single-point turbulence closures. In: Hallbäck, M., Henningson, D., Johansson, A., Alfredsson, P. (Eds.), Turbulence and Transition Modelling. Kluwer Academic Publishers, Dordrecht.

Shir, C., 1973. A preliminary study of atmospheric turbulent flows in the idealized planetary boundary layer. J. Aim. Sci. 30, 1327–1339.

Sloan, D., Smith, P., Smoot, L., 1986. Modeling of swirl in turbulent flow systems. Prog. Energ. Combust. Sci. 12, 163–250.

Spalart, P., 2000. Strategies for turbulence modelling and simulations. Int. J. Heat Fluid Flow 21 (3), 252–263.

Syred, N., Beer, J., 1974. Combustion in swirling flows: A review. Combust. Flame 23, 143–201.

Tang, G, Yang, Z., McGuirk, J., 2002. Large eddy simulation of isothermal confined swirling flow with re-circulation. In: Rodi, W, Fueyo, N. (Eds.), Engineering Turbulence Modelling and Experiments 5. Elsevier Science Ltd., pp. 885–894.

Wallin, S., Hellsten, A., Schatz, M., Rung, T., Peshkin, D., Johansson, A., 2003. Streamline curvature corrected algebraic Reynold's stress turbulence modelling. In: Third International Symposium on Turbulence and Shear Flow Phenomena, vol. 1. pp. 45–50.

Wegner, B., Kempf, A., Schneider, C., Sadiki, A., Dreizler, A., Janicka, J., Schäfer, M., 2004. Large eddy simulation of combustion processes under gas turbine conditions. Prog. Comput. Fluid Dyn. 4, 257–263.